NANOSYSTEMS:
PHYSICS, CHEMISTRY, MATHEMATICS

Adam I.A., et al. *Nanosystems: Phys. Chem. Math.*, 2022, **13** (4), 392–403.
http://nanojournal.ifmo.ru
DOI 10.17586/2220-8054-2022-13-4-392-403

Original article

Comparison of Gaussian and vortex beams in free-space QKD with phase encoding in turbulent atmosphere

Iurii A. Adam[a], Daniil A. Yashin[b], Daria A. Kargina[c], Boris A. Nasedkin[d]

ITMO University, St. Petersburg, 197101, Russia

[a]adam_yura@mail.ru, [b]dayashin@itmo.ru, [c]dakargina17@gmail.com, [d]b.nasedkin@bk.ru

Corresponding author: Iurii A. Adam, adam_yura@mail.ru

PACS 03.67.Dd, 42.25.Dd

ABSTRACT At present, free-space QKD systems are being actively researched and developed. The main limitation of these systems remains the strong influence of atmospheric turbulence and weather conditions on the propagating Gaussian beam. In turn, a number of works have shown that vortex beams are more stable in a turbulent atmosphere. Thus, in this work, the use of vortex beams in the free-space QKD system with phase encoding under the condition of a turbulent atmosphere and their comparison with Gaussian beams are studied. The possibility of phase modulation preservation with additional modulation and demodulation of the vortex beam is also investigated.

KEYWORDS quantum key distribution, vortex beam, atmospheric turbulence, free-space, phase encoding, fork-grating

ACKNOWLEDGEMENTS The study is funded by RPMA grant of School of Physics and Engineering of ITMO University. The authors of this work express their gratitude to Aleksey Viktorovich Chernykh from ITMO University for his support and discussions during the experiment, to Artur Mukhamadiev for his help with illustration preparation and to the Centre for Reprography at the Russian National Library for the production of the fork-gratings.

FOR CITATION Adam I.A., Yashin D.A., Kargina D.A., Nasedkin B.A. Comparison of Gaussian and vortex beams in free-space QKD with phase encoding in turbulent atmosphere. *Nanosystems: Phys. Chem. Math.*, 2022, **13** (4), 392–403.

1. Introduction

Quantum key distribution (QKD) is a new direction in communication technology. QKD establishes the secure connection between two parties (usually called Alice and Bob), where the reliability of purposed channel is provided by the laws of quantum mechanics, the most important of which is no-cloning theorem [1]. In the long run, QKD provides safer connection than common cryptosystems based on the complexity of calculating mathematical functions.

The first proposed protocol was BB84 [2], where the secret key was generated by using two orthogonal photon polarization bases. Since that time, many protocols and experimental schemes were investigated to improve the parameters of QKD systems and expand the possibilities of their applications [3]. In particular, free-space QKD has been actively developed due to its flexibility and mobility which can be used in mobile devices [4], satellite communication [5] and Internet of Things (IoT) [6]. Despite its advantages, free-space QKD has not been widely used in commercial systems compared to optical fiber ones. The main limitation of these systems is the deviation of the Gaussian beam from the original direction of propagation resulting from atmosphere turbulence and weather conditions. To solve this problem, telescopic systems with a large entrance aperture or special correction systems are currently used, which increase the complexity, weight and cost of QKD systems.

As an alternative method of beam deviation compensation, optical vortices can be used, which, according to a number of studies [7, 8], are more stable in a turbulent atmosphere. Optical vortices, or optical radiation with orbital angular momentum (OAM), have a spatial singularity at their center, where the phase remains indeterminate, and along the inner edges of the beam varies from 0 to 2π [9]. The number of these transitions corresponds to the topological charge of the vortex. At present, vortex beams have already been studied in QKD systems, in particular, as bases for encoding information [10] and for multiplexing a channel with respect to the orbital momentum [11]. However, no comparison has been made between the propagation of Gaussian and vortex beams in a free-space QKD with turbulent atmosphere and their influence on the parameters of such systems. Also, no experimental studies have been carried out on the phase modulation preservation with additional modulation and demodulation of the vortex beam, which is necessary for the effective integration of the atmospheric channel with the optical fiber. These questions will be explored in this article.

2. Theory

2.1. Beam Propagation

Analytical expression for the electric field of Laguerre-Gaussian modes, well-known example of vortex beams shown in Fig. 1, is given in the form [12]:

$$u(r,\phi,z) = E_0 \left(\sqrt{2}\frac{r}{w(z)}\right)^l L_p^l \left(2\frac{r^2}{w(z)^2}\right) \frac{w_0}{w(z)} \exp\left[-i\varphi_{pl}(z)\right] \exp\left[i\frac{k}{2q(z)}r^2\right] \exp(il\phi), \tag{1}$$

where L_p^l is the Laguerre polynomial corresponding to the given mode, $q(z)$ is the complex beam parameter, $w(z)$ is the beam radius, w_0 is the waist radius, $\varphi_{pl}(z) = (2p + l + 1)\tan^{-1}(z/z_0))$ is the Gouy phase shift, $z_0 = \pi w_0^2/\lambda$ is the Rayleigh length, $k = 2\pi/\lambda$ is the wave number, λ is the radiation wavelength, r is the radial coordinate of the cylindrical coordinate system. Indices p and l denote radial and azimuth numbers of the mode respectively (the latter is also called the topological charge). Using expression (1), one can obtain the desired distributions, as well as the beam intensity profiles. Since the Gaussian beam is the Laguerre - Gaussian zero mode, one can obtain an analytical expression for the Gaussian beam by setting $l = 0, p = 0$ in (1).

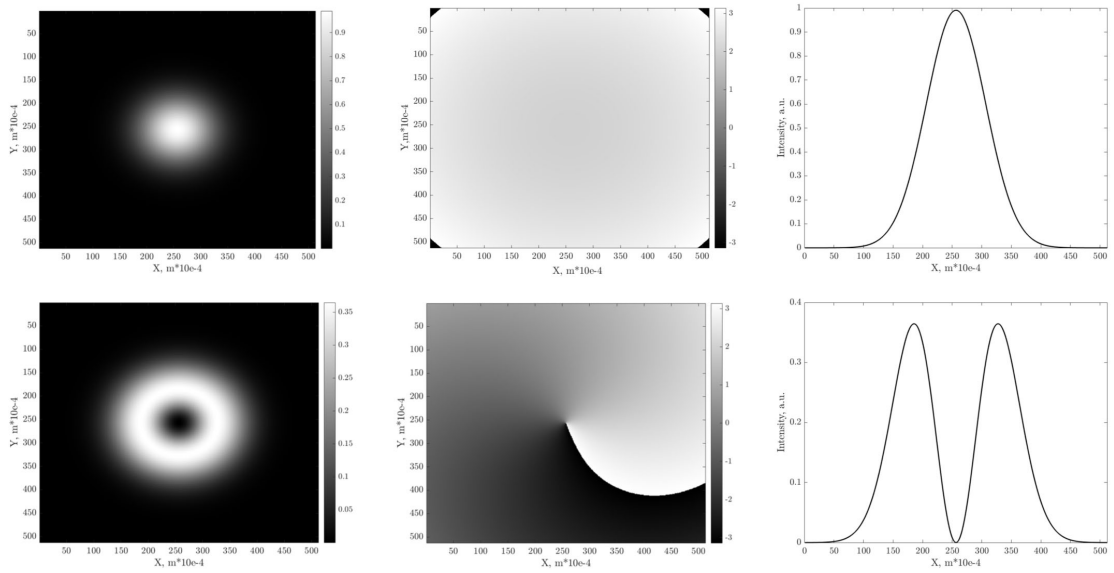

FIG. 1. Laguerre-Gaussian modes. Columns show intensity distributions, phase fronts and beam profiles of Gaussian beam (Top) and Laguerre-Gaussian first mode (Bottom)

Modeling of free space vortex beams propagation is made by using multiple random phase screens method [13], general scheme of which is shown in Fig. 2. In this method, the simulation of turbulence is carried out by placing on the propagation path many thin phase screens, dividing this path into a certain number of segments, on each of which the medium can be considered homogeneous. Thickness is a key point, since in the phase screen approximation, its effect extends only to the radiation phase, the amplitude does not change. The propagation of radiation in a segment of a homogeneous medium can be described by using the calculation of diffraction by the Rayleigh-Sommerfeld method:

$$U_2(x,y) = \frac{z}{j\lambda} \iint_\Sigma U_1(\xi,\eta) \frac{\exp(jkr_{12})}{r_{12}^2} d\xi d\eta, \tag{2}$$

where z is the distance between the centers of the source and receiver planes, r_{12} is the distance between the source and the observation points, ξ, η are the integration variables, Σ is the source area.

Expression (2), in the general case, is a superposition integral, but for planar geometry, in which the source and receiver planes are parallel, it becomes a convolution-type integral

$$U_2(x,y) = \iint U_1(\xi,\eta) h(x-\xi, y-\eta) d\xi d\eta \tag{3}$$

Applying the convolution theorem, we obtain from (3):

$$U_2(x,y) = \mathfrak{F}^{-1}\left\{\mathfrak{I}\left\{U_1(x,y)\right\} H\left(f_X, f_Y\right)\right\}, \tag{4}$$

where the transfer function H is as follows:

$$H\left(f_X, f_Y\right) = e^{jkz} \exp\left[-j\pi\lambda z\left(f_X^2 + f_Y^2\right)\right] \tag{5}$$

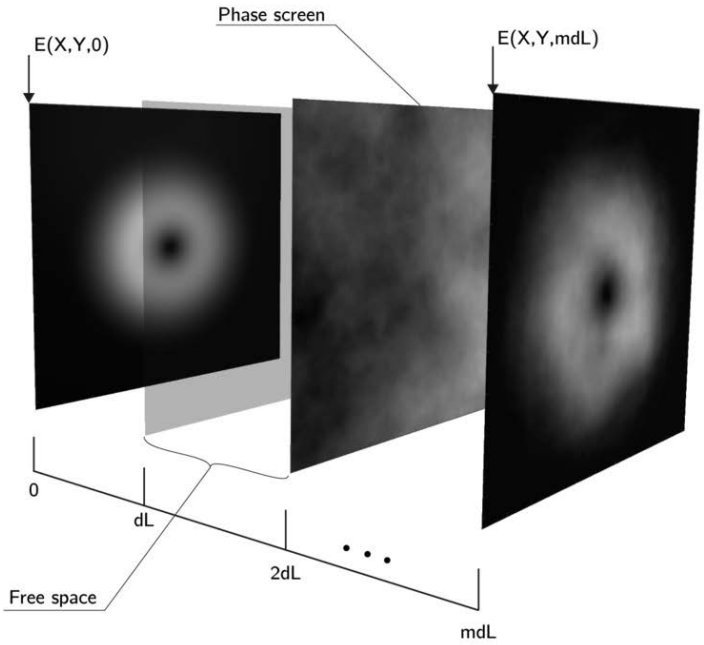

FIG. 2. Scheme of the method of many phase screens for modeling the propagation of radiation in a randomly inhomogeneous medium

2.2. Turbulence and scattering effects

After passing through the homogeneous section of the channel, the beam passes through the phase screen. The effect of the phase screen on the radiation is reduced to the usual multiplication by the exponential term:

$$U_{\text{in}}\ (x, y, z_+) = U_{\text{in}}\ (x, y, z_-) \cdot \exp[i \cdot \varphi(x, y).] \tag{6}$$

The z_+ and z_- coordinates correspond to the field after and before passing through the screen, respectively. Here $\varphi(x, y)$ is the spatial distribution of the random phase, which is a characteristic of some spectrum of the random phase. In this work, the von Karman-type power spectrum of the random phase was used [14]:

$$\Phi(\boldsymbol{\kappa}) = \frac{C(\alpha) r_C^{-\alpha}}{\left(\kappa^2 + \kappa_0^2\right)^{1+\alpha/2}} \exp\left(-\frac{\kappa^2}{\kappa_m^2}\right), \tag{7}$$

$$C(\alpha) = \frac{\alpha 2^{\alpha-2}\Gamma(1+\alpha/2)}{\pi\Gamma(1-\alpha/2)},$$

where $\kappa_0 = 2\pi/L_0$, $\kappa_m = 2\pi/l_0$, $1 < \alpha < 2$, $\Gamma(1 \pm \alpha/2)$ is the Euler Gamma-function, L_0 is the outer scale of turbulence, l_0 is the inner scale of turbulence, r_C is the atmosphere coherence length.

The radiation power loss in the communication channel can be described by the Bouguer - Lambert - Beer law:

$$I(\lambda, z) = I_0(a) \exp\left(-z\alpha_{ext}(\lambda)\right), \tag{8}$$

where $\alpha_{ext}(\lambda)$ is the extinction coefficient. This coefficient consists of two components - the attenuation coefficients due to absorption and scattering:

$$\alpha_{ext}(\lambda) = \alpha_{abs}(\lambda) + \alpha_{scatt}(\lambda)$$

Taking into account the wavelength range in which the system is modeled (the telecommunications range (λ = 1500 nm)), the atmospheric absorption coefficient can be neglected, since its contribution to the total attenuation coefficient is insignificantly small [15].

As for the scattering coefficient, it is the sum of the coefficients of the Rayleigh scattering and the Mie scattering. It is known from theory that the energy loss due to Rayleigh scattering is inversely proportional to the fourth power of the wavelength:

$$\sigma_{\text{s}} = \frac{2\pi^5}{3}\frac{d^6}{\lambda^4}\left(\frac{n^2-1}{n^2+2}\right)^2, \tag{9}$$

where d is the diameter of the molecule, n is the refractive index of the medium, and λ is the radiation wavelength. Given this fact, for the telecommunications wavelength range, the molecular scattering coefficient can be neglected.

Mie scattering occurs on particles whose size is of the order of the radiation wavelength. Typical size of the components of atmospheric aerosols varies greatly and ranges from 10^{-9} m to 10^{-5} m. Since the estimation of the Mie

scattering coefficient requires knowledge of the concentration and distribution of particles, which is an experimentally difficult problem. There are models that describe aerosol conditions depending on the meteorological or local characteristics of the environment. Thus, the signal attenuation caused by Mie scattering can be estimated using the dependence of the attenuation coefficient on the visibility range of objects through the atmosphere [15, 16].

$$\alpha_{scatt}(\lambda) = \frac{3.91}{V}\left(\frac{\lambda}{550}\right)^{-\delta}, \tag{10}$$

$$\delta = \begin{cases} 1.6, & V > 50 \text{ km}; \\ 1.3, & 6 \text{ km} < V < 50 \text{ km}; \\ 0.585\, V^{1/3}, & V < 6 \text{ km}. \end{cases} \tag{11}$$

2.3. Random phase screen generation procedure

We use trigonometric representation of random phase simulation algorithm:

$$\psi(\mathbf{r}) = \sum_{n=1}^{N} a_n \exp\left(i\mathbf{k}_n \cdot \mathbf{r}\right), \quad \varphi_1(\mathbf{r}) = \mathrm{Re}[\psi(\mathbf{r})], \quad \varphi_2(\mathbf{r}) = \mathrm{Im}[\psi(\mathbf{r})], \tag{12}$$

where $\psi(r)$ is the complex phase, $r(x, y)$ is the point at which the phase is calculated, a_n are the random complex spectral amplitudes, $k_n(p_n, q_n)$ are the wave vectors of the individual spectral components, N is the number of spectral components used to represent the complex phase. The method for generating phase screens is based on the discrete Fourier transform of the phase [14]:

$$\psi_{DFT}(j\Delta x, l\Delta x) = \sum_{m,n=-N_{DFT}/2}^{N_{DFT}/2-1} a_{m,n} \exp\left(\frac{2i\pi}{N_{DFT}}(mj + nl)\right), \tag{13}$$

where $\Delta x = L/N_{DFT}$, $\Delta k = 2\pi/L$. The structural function of such phase has the form:

$$D_{DFT}(j\Delta x, l\Delta x) = 2(\Delta k)^2 \sum_{m,n=-N_{DFT}/2}^{N_{DFT}/2-1} \Phi(m\Delta k, n\Delta k)\left[1 - \exp\left(\frac{2i\pi}{N_{DFT}}(mj + nl)\right)\right], \tag{14}$$

where $\Phi(m\Delta k, n\Delta k)$ is the spatial phase spectrum corresponding to the chosen von Karman turbulence model. An example of a generated phase screen is shown in Fig. 3.

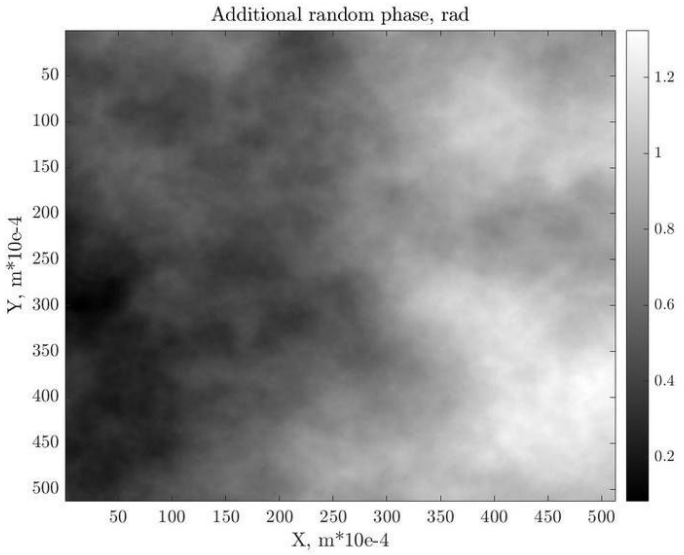

FIG. 3. An example of a generated random phase screen according to the selected turbulence spectrum

2.4. QKD system parameters estimation

As the object of study the subcarrier wave quantum key distribution (SCW QKD) system were chosen [17], the free-space implementation of which is described in [15]. The study of the parameters of this system, as well as their description, are detailed in [18].

It is worth noting that the propagation of quantum signals from the sender to the receiver is considered in the approximation of the classical description. In this article we do not consider the quantum effects such as quantum entanglement, quadrature and photon number squeezing, precisely described in [19, 20]. This approximation was made on the basis of the fact that the protocol used in the SCW QKD system is based on the use of attenuated laser pulses - coherent states (obeying Poisson statistics), which are not strictly single-photon states (constituting the Fock basis).

One of the main values, characterizing a QKD system is the secret key generation rate:

$$K\left(\mu_0, m, L\right) = \frac{1-G}{2T}\left[1 - h\left(\frac{E}{1-G}\right) - h\left(\frac{1}{2}\left(1 - e^{-\mu_0(1-J_0(2m))}\right)\right)\right], \tag{15}$$

where

$$E = \frac{1}{2}P_{det}(0, \pi + \Delta\varphi), \tag{16}$$

$$1 - E - G = \frac{1}{2}P_{det}(0, \Delta\varphi), \tag{17}$$

$$h(Q) = -Q\log_2 Q - (1-Q)\log_2(1-Q), \tag{18}$$

$$Loss = 10\log(\frac{P_{in}}{P_{out}}), \tag{19}$$

$m = \sqrt{m_A^2 + m_B^2 + 2m_A m_B \cos\left(\varphi_A - \varphi_B\right)}$ is the modulation index of the system, where m_A, m_B are modulation indices in Alice's and Bob's modules respectively, $h(Q)$ is the binary Shannon entropy, T is the pulse duration, μ_0 is the average number of photons at the input of Alice's modulator, L is the length of the communication channel, P_{in} is the power at the source plane, P_{out} is the power at the detector plane. The value $P_{det}(0, \pi + \Delta\phi)$ or $P_{det}(0, \Delta\phi)$ in (16), (17) represents the probability of detecting a photon in the recipient block

$$P_{det}\left(\varphi_A, \varphi_B\right) = \left(\eta_D \frac{n_{ph}\left(\varphi_A, \varphi_B\right)}{T} + \gamma_{dark}\right)\Delta t, \tag{20}$$

where φ_A, φ_B are the phase delays introduced in the modulators of Alice and Bob, respectively, η_D is the quantum efficiency of the detector used, γ_{dark} is the frequency of dark counts, Δt is the detector gating time. The average number of photons arriving at Bob's detector in time T:

$$n_{ph}\left(\varphi_A, \varphi_B\right) = \mu_0\eta(L)\eta_B\left(1 - (1-\vartheta)\left|J_0\left(m\right)\right|^2\right), \tag{21}$$

where η_B is the loss in the Bob's module, ϑ is the coefficient that takes into account the imperfection of spectral filtering in the recipient block, J_0 is the Bessel function of the first kind.

Another equally important characteristic is the quantum bit error rate (QBER):

$$Q(L) = \frac{E}{1-G}. \tag{22}$$

QBER represents the ratio of a negative outcome probability - an error of detection, to the probability of obtaining any outcome.

3. Numerical results

3.1. Beam propagation

Modeling the process of radiation propagation in a turbulent atmosphere contains several stages. At the initial stage, it is necessary to obtain intensity distributions, phases, as well as intensity profiles of both beams in the source plane - at the exit from the Alice's module. In this work, the process of generation of vortex radiation is not considered, and the simulation of its direct propagation begins after the vortex beam has already been obtained. Modeling of Gaussian beam is carried out with the use of the following parameters: λ = 1500 nm; ω_0 =1 cm ; z_0 = 20 m; $l = 0$, $p = 0$. Parameters for vortex beam are λ = 1500 nm; ω_0 =1 cm ; z_0 = 20 m; $l = 1$, $p = 0$. Results of the first stage are shown in Fig. 1.

Further, having the input characteristics of the beams, it is necessary to carry out the procedure for their propagation over a given distance. At the input of the propagation channel, just behind the input plane, a random phase screen is placed, generated by an algorithm based on the discrete Fourier transform of a random phase, mentioned above and described in detail in [14]. A random phase screen affects the phase front of the original beam, distorting it. We numerically investigated two cases: r_C = 1 m; r_C = 0.1 m. The shorter coherence length corresponds to a stronger turbulence. Other chosen parameters of the atmosphere are: l_0 = 1 cm; L_0 = 10 m; $\alpha = \frac{5}{3}$; V = 20 km. Total channel length on this stage was L = 1000 m, the propagation results of which are shown in Fig. 4. Distance between the phase screens

ΔL is chosen to be 100 m, (i.e. 11 phase screens are used), as it is typical distance for this kind of simulation [21]. Aperture of the receiving telescope is D_{det}^{G} = 0.17 m for the Gaussian beam and D_{det}^{V} = 0.20 m for the vortex beam. Aperture diameters remain constant for all the propagation distances. The difference between aperture diameters of the receiving telescopes is dictated by the fact that the studied beams have different cross-sectional areas for equal waist radii. Since the purpose of this study is to compare the considered beams under the same conditions, we chose apertures of the receiving telescopes that would provide the same ratio of the cross-sectional areas of the beams and the areas of the detectors (receiving telescopes). Fig. 4 shows the case, where the beam, propagating through a turbulent atmosphere, undergoes shape distortions, as well as phase front distortions. This distortion is the stronger, the shorter the atmosphere coherence length is. Also, it can be seen that with an increase of turbulence strength, the shift of the beam center relative to the given axis of its propagation becomes more obvious, this phenomenon is called beam wandering. These "wanders", depicted in Fig. 5, lead to geometric losses of radiation, since the beam goes beyond the boundaries of the aperture of the receiving telescopic device. Table 1 shows the average values of the shifts and root-mean-square deviations of the shifts of both beams as they propagate through the turbulent channel at distance L = 1000 m. To perform this assessment, 30 independent simulations were carried out.

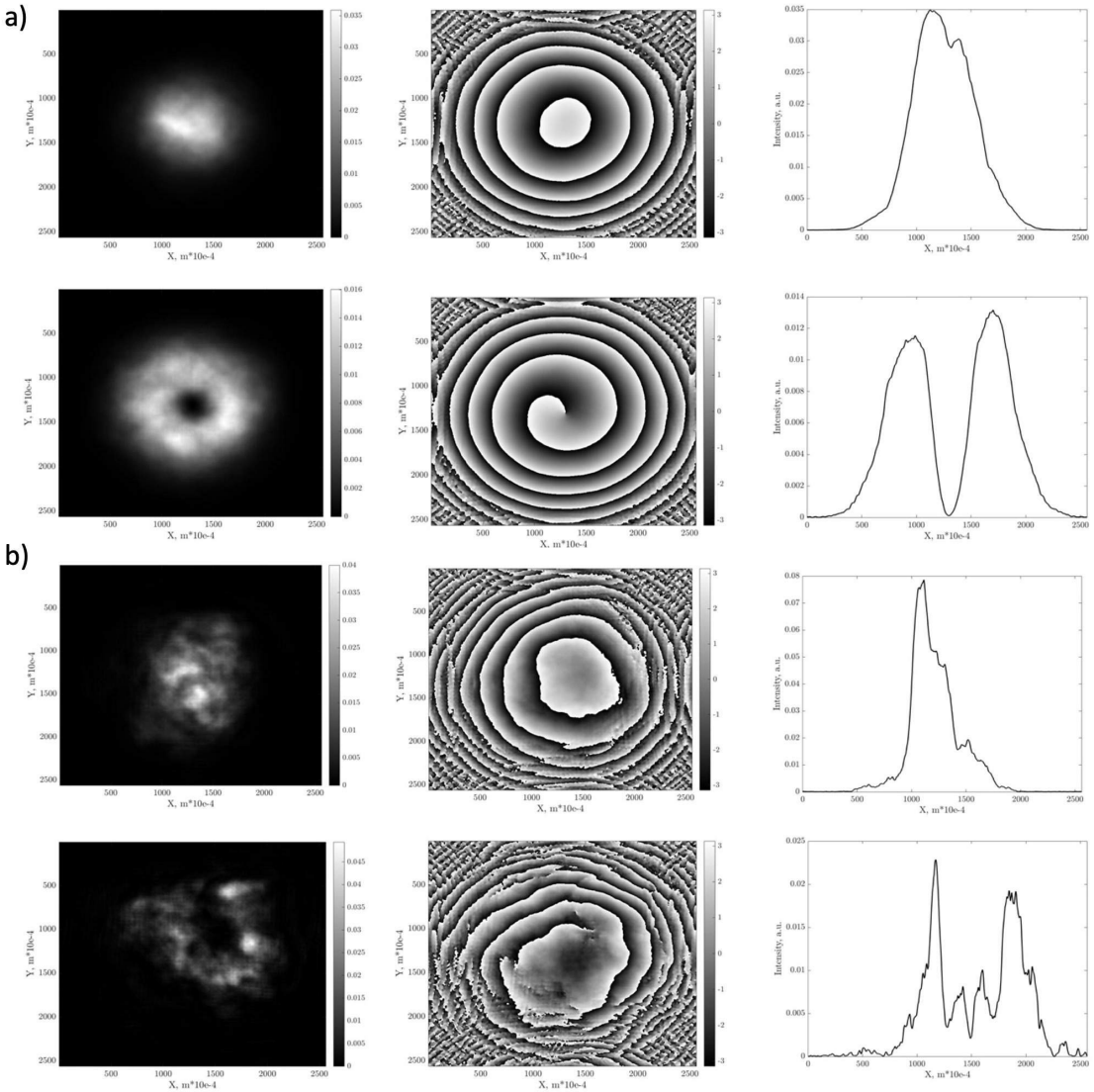

FIG. 4. Intensity distribution, phase distribution and intensity profile in the detector plane of Gaussian beam and vortex beam at the distance L = 1000 m from the source plane in case of a) r_C = 1 m; b) $r_C = 0.1$ m

The achieved values can serve as a measure of beam stability during propagation in a turbulent atmosphere. It is shown that the vortex beam experiences a smaller average deviation compared to the Gaussian beam under turbulence conditions, and the values of the standard deviation of the shift indicate that the area of the region within which the vortex beam will be located is less than for the Gaussian beam. The loss of optical radiation power that beams experience

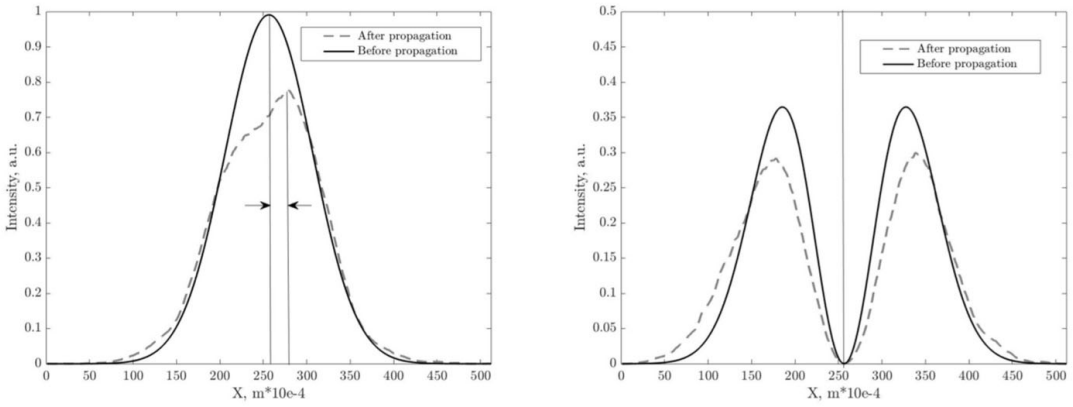

FIG. 5. Shift of beams' centers due to turbulence

TABLE 1. The results of the study of the shift of the centers of the Gaussian and the vortex beams during propagation through a turbulent atmosphere at distance L = 1000 m

	r_C, m	Average shift, mm	RMS shift deviation, mm
Gaussian Beam	1	8.5	±6.5
Vortex Beam	1	3.3	±1.2
Gaussian Beam	0.1	47.5	±25.6
Vortex Beam	0.1	19.2	±12.0

when propagating in a turbulent communication channel can be calculated from the knowledge of the beam intensity distributions in the source and detector planes. In this paper, the power is calculated using the Simpson's method. Optical loss in dB can be calculated using formula (19). The obtained value of losses contains the contribution caused by the influence of Mie scattering, this contribution can be calculated using formulas (11), (12). When calculating losses due to Mie scattering, the parameters for atmospheric visibility V = 20 km were used. A comparison of the radiation loss in the communication channel for Gaussian and vortex beams is shown in Fig. 6. The graphs show that the vortex beams experience lower losses in the communication channel for given values of the atmospheric coherence length. The average loss at the distance L = 1000 m with r_C = 0.1 m for the vortex beam is by 0.2 dB less than for the Gaussian beam.

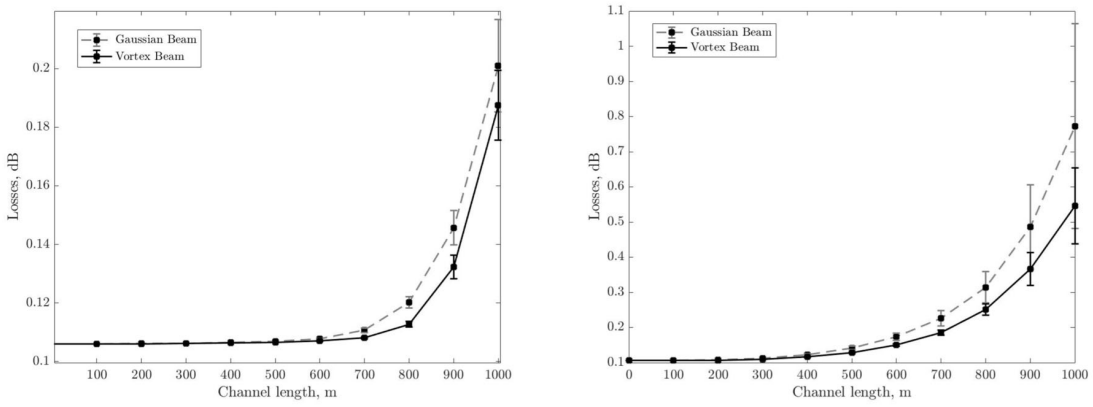

FIG. 6. Dependence of radiation losses in an atmospheric communication channel on its length for $r_C = 1$ m (Left) and $r_C = 0.1$ m (Right)

3.2. QKD parameters

Using the obtained values of losses in the communication channel, we can calculate the average number of photons arriving at Bob's detector (21), the probability of detecting a photon in the receiver unit (20), as well as the key generation

rate (15) - (18) and QBER (22). When calculating the characteristics of the QKD system, the following parameters were used [18]: T = 10 ns ,υ_S = 100 MHz, m = 0.319, μ_0 = 4, $\Delta\phi = 5^\circ$, $\eta_B = 10^{-0.64}$, $\vartheta = 10^{-3}$, γ_{dark} = 20 Hz, η_D = 0.2. The results of numerical calculation of the key generation rate and the quantum bit error rate for r_C = 1 m and r_C = 0.1 m are shown in Fig. 7, 8, respectively.

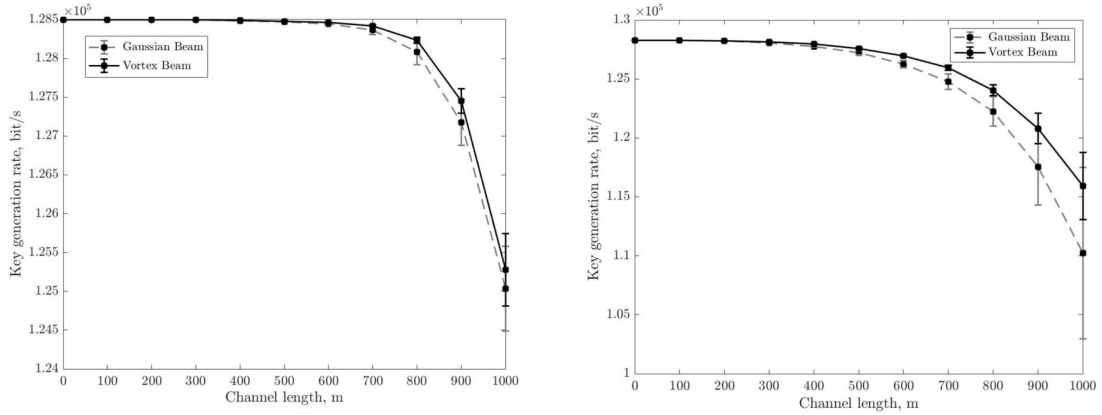

FIG. 7. Dependence of key generation rate in an atmospheric communication channel on its length for r_C = 1 m (Left), r_C = 0.1 m (Right)

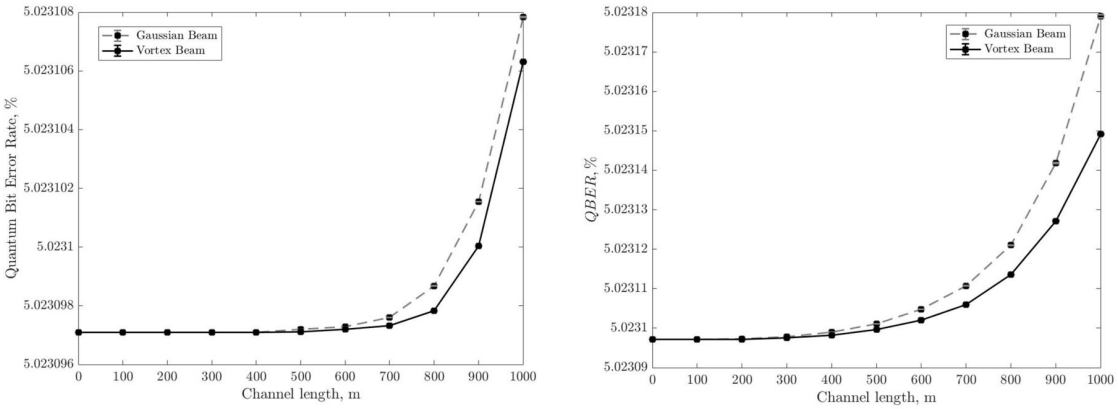

FIG. 8. Dependence of QBER in an atmospheric communication channel on its length for r_C = 1 m (Left), r_C = 0.1 m (Right)

These results are in good agreement with the beam wandering and the channel losses estimates. Since the key generation rate and QBER are related to the losses in the communication channel, it is natural that there is a slight advantage with respect to these parameters as well. For r_C = 1 m, the numerical curves for the key generation rate and QBER are almost indistinguishable: the difference of mean values for given beams is small and the standard deviation values are nearly equal, despite the fact that the vortex beam shows slightly better results. However, more significant advantage can be seen for r_C = 0.1 m. The average key generation rate for the vortex beam is about 5% higher than for the Gaussian beam at L = 1000 m and its standard deviation is noticeably less. Numerical results for QBER, however, shows less difference between the Gaussian and the vortex beams, but may be more significant at longer distances, which requires further studies.

4. Experiment

To study the possibility of phase modulation preservation during the transition from the Gaussian to the vortex beam and vice versa in the QKD system with phase coding, an experimental setup was implemented. The purposed scheme is a classic Mach-Zehnder interferometer, in one of the arms of which modulation and demodulation of the vortex beam were performed. It is important to clarify that the proposed scheme is not a full-fledged QKD system, but it only imitates the process of phase coding in the classical approximation, however, the results obtained in this work will also be valid for a full-fledged quantum communications system.

Currently, to generate vortex beams, the following methods are used: spiral phase plate [22], fork-grating [23] and spatial light modulators (SLM) [24]. In this work, the method of fork-grating was used as the most accessible and inexpensive one. Fork-grating is a diffraction grating in the middle of which a spatial dislocation is located. Mathematically it can be obtained as an interference pattern of a vortex beam and an inclined plane wave. In order to use such gratings in an experimental setup, the pictures with required fork-gratings obtained by mathematical modeling were printed in high resolution and then transferred to a 35 mm film using the reprography method. As a result of the interaction of a Gaussian beam with such fork-gratings, vortex beams are generated in side diffraction orders, the topological charge of which coincides with the order number. Demodulation of the vortex beam in this case is provided by using a second symmetrical fork-grating rotated by 180 degrees, which makes it possible to obtain a Gaussian beam in the same diffraction order as the vortex beam on the first fork-grating. The profiles of the obtained beams is illustrated in Fig. 9. The results obtained confirm the modulation and demodulation of the vortex beam; nevertheless, the resulting demodulated Gaussian beam has residual vortex components, which can be explained by the non-ideal alignment and broadening of the singularity of the vortex beam during propagation, which leads to its incomplete compensation on the second fork-grating.

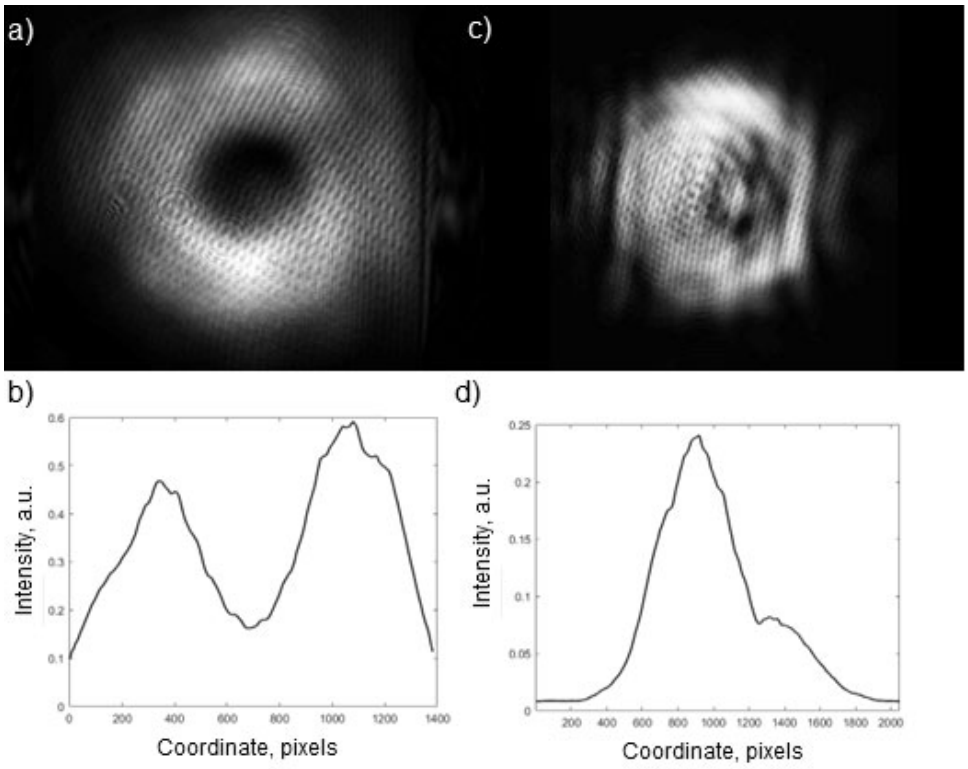

FIG. 9. (a) Profile of a vortex beam modulated on the fork-grating; (b) cross section of the modulated vortex beam; (c) profile of the Gaussian beam demodulated on the fork-grating; (d) cross section of the demodulated Gaussian beam

In the purposed scheme shown in Fig. 10, the He-Ne laser module (LM) with the wavelength of 633 nm were used. This wavelength has already been used in several works on free-space QKD [4, 25, 26] due to the simplification of the alignment process. The optical radiation was directed to the beamsplitter (BS1), after which the first laser beam entered the phase modulator (PM), where it acquired a delay of 0 or π radians, and the second laser beam by the mirror (M1) was directed to beamsplitter (BS2) on the exit of interferometer. Next, the first beam went through the described above process of modulation and demodulation of the optical vortex on two fork-gratings (FG1 and FG2). The distance between these gratings was 42 cm and the first-order diffraction angle was 1.8 degrees. As a result, the obtained demodulated Gaussian beam by the mirror (M2) was directed to beamsplitter (BS2) on the exit of interferometer, where it interfered with the second beam. The interference pattern was recorded using camera (C) placed at one of the outputs of the beamsplitter (BS2). The intensity profiles of the obtained interference patterns at different values of the phase delay, which were additionally averaged over 60 frames to compensate the phase fluctuations in the interferometer, are shown in Fig. 11. From the obtained results, it can be seen that the value of the introduced phase delay is equivalently reflected in the recorded interference pattern. As a result, it can be concluded that the process of modulation and demodulation of the optical vortex does not affect the process of phase encoding and can be used in the QKD systems with phase encoding.

It is necessary to make important remarks on the obtained experimental results. Firstly, in this work there is a certain discrepancy between the theoretical model and the experimental scheme. It lies in the fact that Laguerre-Gaussian modes were used to describe the vortex field in the mathematical model, while in the experimental scheme the vortex beams

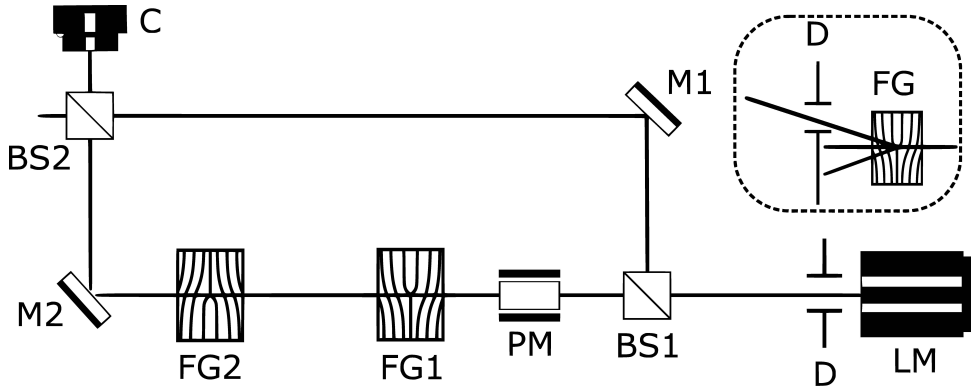

FIG. 10. Mach-Zehnder interferometer on demodulated vortex beam; (in the dotted frame) selection of the first order diffraction on fork-grating

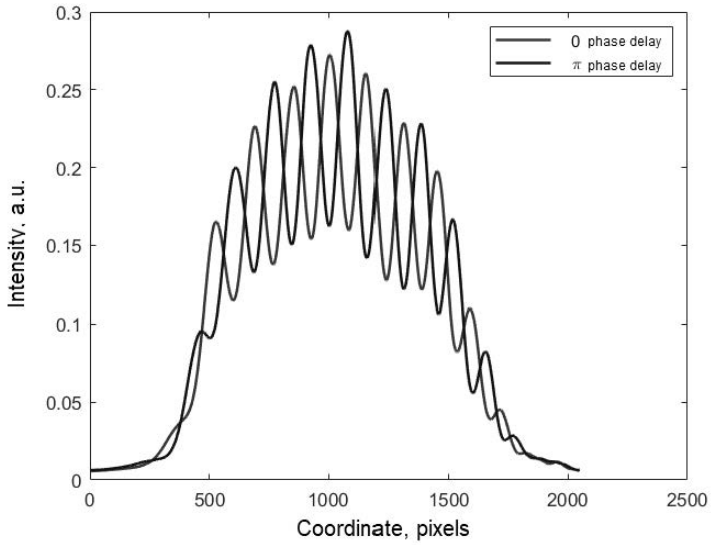

FIG. 11. Cross section of the interference pattern at a phase delay of 0 and π radians, averaged over 60 frames

were modulated on fork-gratings, which, in fact, is described by the Kummer beams [27]. However, this discrepancy is not crucial and does not affect the obtained results, since the theoretical model considers the parameters of the SCW QKD system, and the experimental scheme considers the possibility of the phase encoding preservation, which does not correlate with each other. Secondly, by using a fork-grating in the SCW QKD, the diffraction angles of the carrier and subcarrier waves will differ by 10^{-4} degrees. This will result in their spatial displacement by 1.7 mm at a distance of 1 km, which is comparable to the atmospheric turbulences deviation in the theoretical model. This problem, like the first one, can be solved by using SLM as a method of generating vortex beams, which will allow one to compensate diffraction angle deviation of the carrier and subcarrier waves, as well as to implement Laguerre-Gaussian modes in the experimental scheme to correlate the theoretical model and experiment.

5. Conclusion

Thus, in this work the possibility of using vortex beams in the free-space QKD system and its comparison with the Gaussian beam were studied as well as the phase encoding preservation possibility. The authors of this paper would like to once again emphasize the theoretical nature of the research and the presented results. For further practical use, additional researches are needed.

A mathematical model of radiation propagation in the form of Gaussian and vortex beams in a turbulent atmosphere is demonstrated and a comparative estimate of the amount of beam wandering is carried out. The radiation power losses were also calculated, including the geometric losses arising due to the deviation of beams from given propagation axis, as well as the losses introduced by the Mie scattering. In addition, based on the calculated values of radiation power losses in the atmospheric communication channel, the parameters of SCW QKD system were estimated using the considered beams. Taking into consideration the obtained values of the average shift and standard deviation of the shift for both beams, we

can conclude that the vortex beam is, indeed, less prone to turbulence wandering in the communication channel. Obtained results also show that the vortex beam is a more favorable information carrier due to lower losses in the communication channel in comparison with the Gaussian beam. Finally, SCW QKD system parameters estimate points that using of vortex beams gives one better results compared to Gaussian beams as well.

In turn, the experimental results confirm the possibility of the phase encoding preservation in the process of modulation and demodulation of the vortex beam. It was shown that the fork-grating method has a number of limitations for its application in the SCW QKD system, in particular, the discrepancy between the theoretical model and experiment, diffraction angle deviation of carrier and subcarrier waves, and large additional losses on the receiver side due to the fork-grating method low efficiency. As an alternative, the use of the SLM method has been proposed.

Despite the approximations that were mentioned in Section 2, it can be argued that the use of vortex modulation in SCW QKD system is reasonable, since the comparison of the behavior of the studied beams during propagation in a turbulent atmosphere was carried out under the same conditions. However, the model presented in this paper needs further development. In the future, it is planned to move to a dynamic turbulence model that takes into account the temporal variability of atmospheric parameters, as well as modeling the direct process of vortex modulation. Also, the usage of the vortex beam in practical SCW QKD system is planned.

References

[1] Wootters W.K., Zurek W.H., The no-cloning theorem, *Physics Today*, 2009, 62(2), P. 76–77.

[2] Bennett C.H., Brassard G., Quantum cryptography: public key distribution and coin tossing. *Proceedings of the International Conference on Computers, Systems and Signal Processing*, 1984, **1**, P. 175–179.

[3] Pirandola S., Andersen U.L., Banchi L., Berta M., Bunandar D., Colbeck R., Englund D., Gehring T., Lupo C., Ottaviani C., Pereira J.L., Razavi M., Shamsul Shaari J., Tomamichel M., Usenko V.C., Vallone G., Villoresi P., and Wallden P., Advances in quantum cryptography. *Advances in Optics and Photonics*, 2020, **12**(4), P. 1012.

[4] Bourgoin J.-P.,. Higgins B.L, Gigov N., Holloway C., Pugh C.J., Kaiser S., Cranmer M., and Jennewein T., Free-space quantum key distribution to a moving receiver. *Optics Express*, 2015, **23**(26), P. 33437.

[5] Liao S.K., Cai W.Q., Liu W.Y., Zhang L., Li Y., Ren J.G., Yin J., Shen Q., Cao Y., Li Z.P., Li F.Z., Chen X.W., Sun L.H., Jia J.J., Wu J.C., Jiang X.J., Wang J.F., Huang Y.M., Wang Q., Zhou Y.L., Deng L., Xi T., Ma L., Hu T., Zhang Q., Chen Y.A., Liu N.L., Wang X.B., Zhu Z.C., Lu C.Y., Shu R., Peng C.Z., Wang J.Y., and Pan J.W., Satellite-to-ground quantum key distribution. *Nature*, 2017, **549**(7670), P. 43–47.

[6] Al-Mohammed H.A. and Yaacoub E., On the Use of Quantum Communications for Securing IoT Devices in the 6G Era. *2021 IEEE International Conference on Communications Workshops, ICC Workshops 2021 - Proceedings*, 2021.

[7] Zhou Y., Zhao J., Braverman B., Pang K., Zhang R., Willner A.E., Shi Z., and Boyd R.W., Multiprobe Time Reversal for High-Fidelity Vortex-Mode-Division Multiplexing over a Turbulent Free-Space Link. *Physical Review Applied*, 2021, **15**(3), P. 1.

[8] Aksenov V.P. and Pogutsa C.E., Fluctuations of the orbital angular momentum of a laser beam, carrying an optical vortex, in the turbulent atmosphere. *Quantum Electronics*, 2008, **38**(4), P. 343.

[9] Shen Y., Wang X., Xie Z., Min C., Fu X., Liu Q., Gong M., and Yuan X., Optical vortices 30 years on: OAM manipulation from topological charge to multiple singularities. *Light: Science and Applications*, 2019, **8**(1).

[10] Sit A., Fickler R., Alsaiari F., Bouchard F., Larocque H., Gregg P., Yan L., Boyd R.W., Ramachandran S., and Karimi E., Quantum cryptography with structured photons through a vortex fiber. *Optics Letters*, 2018, **43**(17), P. 4108.

[11] Qu Z. and Djordjevic I.B., High-speed free-space optical continuous-variable quantum key distribution enabled by three-dimensional multiplexing. *Optics Express*, 2017, **25**(7), P. 7919.

[12] Soskin M. and Vasnetsov M., Singular optics. *Progress in optics*, 2001, **42**(4), P. 219–276.

[13] Liu Y., Zhang K., Chen Z., and Pu J., Scintillation index of double vortex beams in turbulent atmosphere. *Optik*, 2019, **181**(November), P. 571–574.

[14] Charnotskii M., Four methods for generation of turbulent phase screens: comparison, 2019, no. November.

[15] Kynev S.M., Chistyakov V.V., Smirnov S.V., Volkova K.P., Egorov V.I., and Gleim A.V., Free-space subcarrier wave quantum communication. *Journal of Physics: Conference Series*, 2017, **917**(5).

[16] Kim I.I., McArthur B., and Korevaar E.J., Comparison of laser beam propagation at 785 nm and 1550 nm in fog and haze for optical wireless communications. *Optical Wireless Communications III*, P. 26–37.

[17] Gleim A., Egorov V., Nazarov Y.V., Smirnov S., Chistyakov V., Banni O.k, Anisimov A., Kynev S., Ivanova A., Collins R., *et al.*, Secure polarization-independent subcarrier quantum key distribution in optical fiber channel using bb84 protocol with a strong reference. *Optics express*, 2016, **24**(3), P. 2619–2633.

[18] Miroshnichenko G.P., Kozubov A.V., Gaidash A.A., Gleim A.V., and Horoshko D.B., Security of subcarrier wave quantum key distribution against the collective beam-splitting attack. *Optics Express*, 2018, **26**, P. 11292.

[19] Vasylyev D.Y., Semenov A., and Vogel W., Toward global quantum communication: beam wandering preserves nonclassicality. *Physical review letters*, 2012, **108**(22), P. 220501.

[20] Faleeva M. and Popov I., Entanglement transmission through turbulent atmosphere for modes of gaussian beam. *Quantum Information Processing*, 2020, **19**(2), P. 1–9.

[21] Cheng W., Haus J.W., and Zhan Q., Propagation of vector vortex beams through a turbulent atmosphere. *Optics express*, 2009, **17**(20), P. 17829–17836.

[22] Hui X., Zheng S., Hu Y., Xu C., Jin X., Chi H., and Zhang X., Ultralow reflectivity spiral phase plate for generation of millimeter-wave OAM beam. *IEEE Antennas and Wireless Propagation Letters*, 2015, **14**, P. 966–969.

[23] Karahroudi M.K., Parmoon B., Qasemi M., Mobashery A., and Saghafifar H., Generation of perfect optical vortices using a Bessel–Gaussian beam diffracted by curved fork grating. *Applied Optics*, 2017, **56**(21), P. 5817.

[24] Pradhan P., Sharma M., and Ung B., Generation of perfect cylindrical vector beams with complete control over the ring width and ring diameter. *IEEE Photonics Journal*, 2018, **10**(1), P. 1–10.

[25] Conrad A., Isaac S., Cochran R., Sanchez D., Wilens B., Gutha A., Rezaei T. , Gauthier D.J. and Kwiat P., Drone-based quantum key distribution: QKD. *Proc. SPIE, Free-Space Laser Communications XXXIII*, 2021, 11678, 116780X.

[26] Hill A.D., Chapman J., Herndon K., Chopp C., Gauthier D.J., and Kwiat P., Drone-based quantum key distribution. *Urbana*, 2017, **51**, P 61801–63003.

[27] Bekshaev A.Y., Karamoch A., Vasnetsov M., Pas' ko V., and Soskin M., Structure of optical vortices produced by holographic gratings with "fork" geometry: Kummer beams. *arXiv preprint arXiv:0906.2619*, 2009.

Submitted 1 June 2022; revised 29 June 2022; accepted 30 June 2022

Information about the authors:

Iurii A. Adam – ITMO University, Kronverkskiy, 49, St. Petersburg, 197101, Russia; adam_yura@mail.ru

Daniil A. Yashin – ITMO University, Kronverkskiy, 49, St. Petersburg, 197101, Russia; dayashin@itmo.ru

Daria A. Kargina – ITMO University, Kronverkskiy, 49, St. Petersburg, 197101, Russia; dakargina17@gmail.com

Boris A. Nasedkin – ITMO University, Kronverkskiy, 49, St. Petersburg, 197101, Russia; b.nasedkin@bk.ru

Conflict of interest: the authors declare no conflict of interest.